Supplement of Atmos. Meas. Tech., 11, 6761–6784, 2018
https://doi.org/10.5194/amt-11-6761-2018-supplement

Atmospheric Measurement Techniques
Open Access

Supplement of

Aerosol optical properties derived from POLDER-3/PARASOL (2005–2013) over the western Mediterranean Sea – Part 1: Quality assessment with AERONET and in situ airborne observations

P. Formenti et al.

Correspondence to: Paola Formenti (paola.formenti@lisa.u-pec.fr)

Table S1. Modal diameter (D_0), geometric standard deviation (σ_0) and effective diameter (D_{eff}) of the log-normal distribution as well as real part of the refractive index (m_r) of the aerosol models over ocean of the POLDER-3 Look-Up Table (LUT). The imaginary part of the refractive index (m_i) is assumed as zero.

Parameters	Fine mode	Spherical coarse mode	Non spherical coarse mode
D_0 (µm)	0.08, 0.16, 0.20, 0.26	1.56	0.90, 1.50
σ_0	0.46	0.69	0.69
D_{eff} (µm)	0.136, 0.272, 0.34, 0.442	5.10	2.96, 4.92
m_r	1.35, 1.45, 1.60	1.33, 1.35, 1.37	1.53

Figure S1. Iterative data inversion procedure to retrieve from airborne observations the aerosol optical depth (AOD, AOD_F and AOD_C) and Angstrom exponent (AE) as measured by POLDER-3. Green boxes indicate the input values from airborne measurements (size distribution, scattering and extinction coefficients) and the initial values of the complex refractive indices estimated from published literature. The iterative steps of the procedure are indicated in the blue boxes. The results of optical calculations (corrected size distribution, scattering and extinction coefficients) are in the orange boxes.

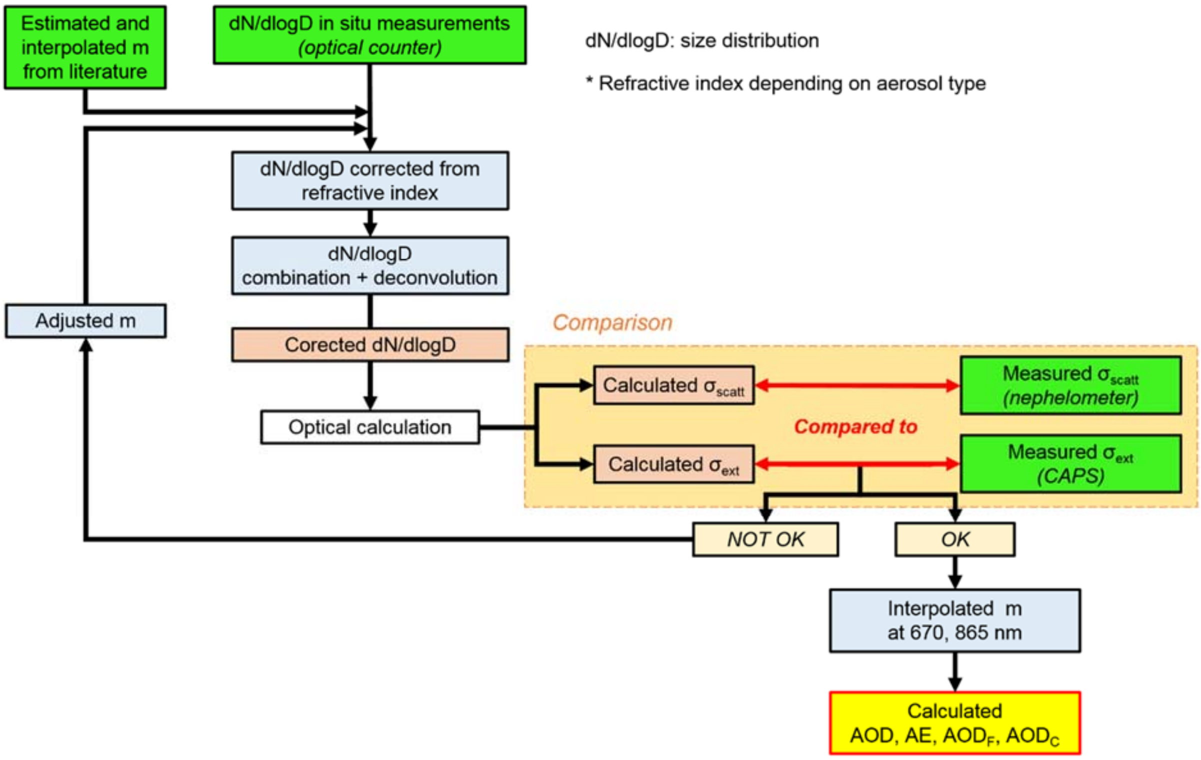

Figure S2. Ratio of the coarse to the total AOD (AOD_C/AOD) by AERONET as a function of the cut-off diameter ($D_{cut\text{-}off}$) between the fine and coarse aerosol particle modes.

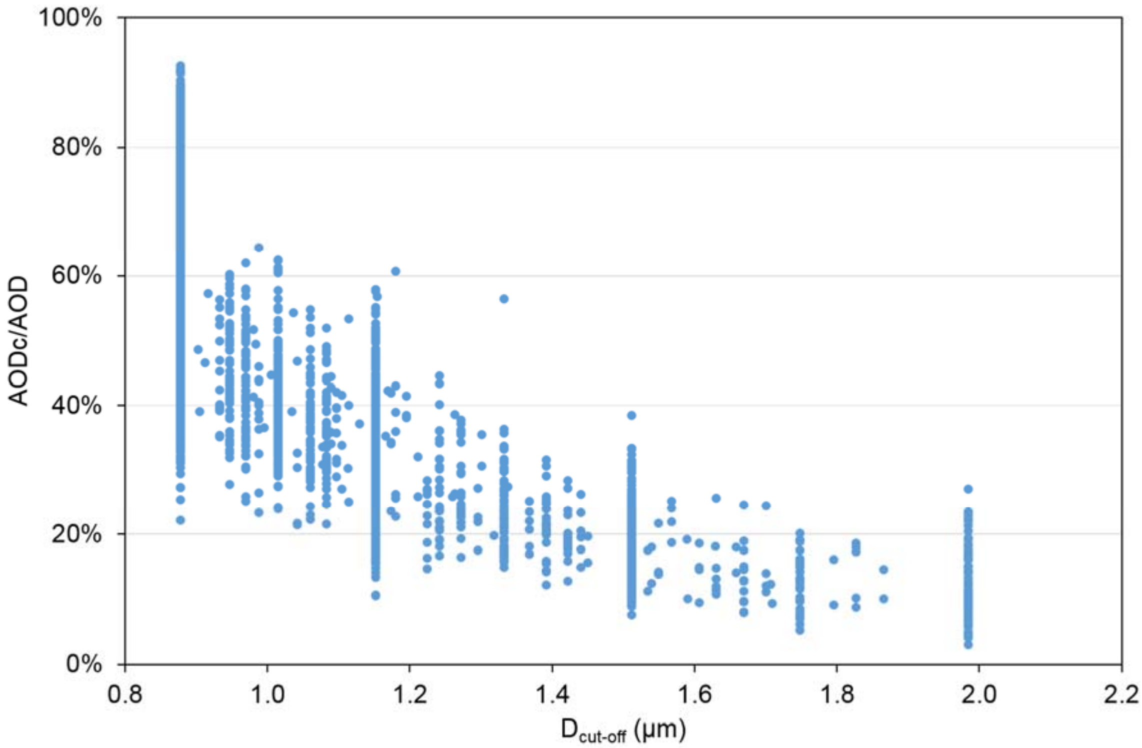

Supplementary A. Assessment of the size distribution

Here we provide details of the procedure to estimate the aerosol particle size distribution from the measurements of the PCASP, UHSAS and Grimm optical counters operated on board the ATR42 during TRAQA and ADRIMED. This also requires to assess the particles complex refractive index.

S.1. Correction for complex refractive index

The operating principle of the particle optical counters is based on the angular dependence of the light scattering intensity to the particle size through optical Mie theory (Mie, 1908; Wendisch and Brenguier, 2013). The optical particle counters provide the number size distribution at an optical equivalent diameter (D_{EO}) corresponding to the measured intensity of the scattered radiation at the value of the complex refractive index *m* used for calibration. This is generally done with latex spheres (or equivalent standard material) for which *m* is equal to 1.59 – i0 at 638 nm. Henceforth, to represent the actual aerosol, the value of D_{EO} needs to be converted into a particle equivalent geometrical diameter (D_{EG}), corresponding to the real value of the complex refractive index. This correction depends on aerosol composition and the geometrical and spectral characteristics of the particle counter (Reid et al., 2003; Denjean et al, 2016).

The equivalence between D_{EO} and D_{EG} was established by calculation using the Mie theory for homogeneous spherical particles (Bohren and Huffman, 1998). Examples of this equivalence for a range of *m* values is shown in Figure S3 for the particle optical counters used in this study (UHSAS, PCASP and Grimm).

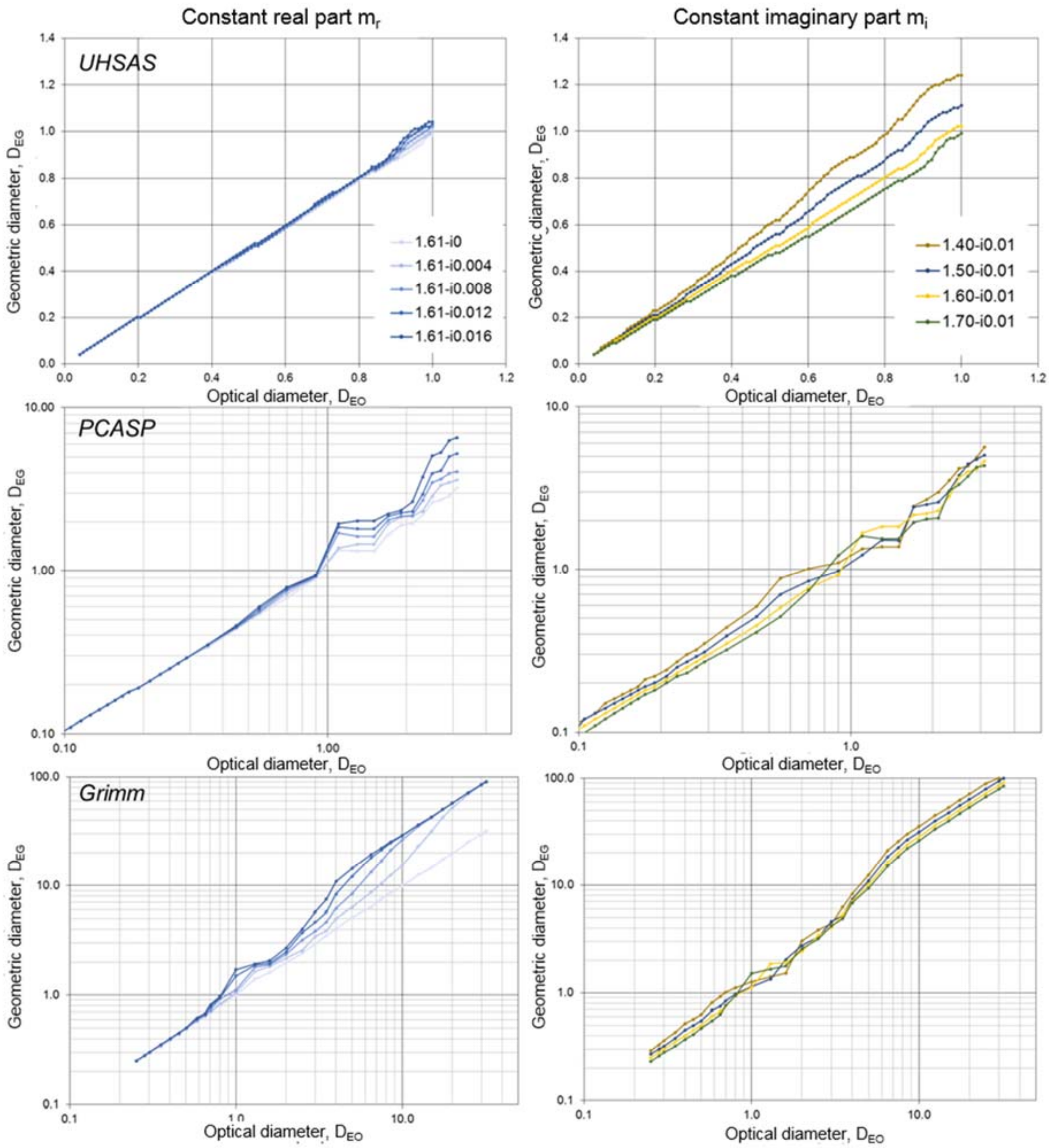

Figure S3. Scatterplot of the geometric-equivalent diameter (D_{EG}) with respect to the optical-equivalent diameter (D_{EO}) for various refractive indices with real part fixed at 1.61 (left) and imaginary part fixed at 0.01 (right), for UHSAS (top), PCASP (middle), and Grimm (bottom).

The relation between D_{EO} and D_{EG} is not linear with size. The real and imaginary parts of the refractive index modify significantly the particle diameter, notably above 0.6 μm. The imaginary part of the refractive index has a greater influence at diameters larger than 1 μm, whereas the real part affects more the submicron aerosols. Figure S3 also shows the equivalence between D_{EO} and D_{EG} is not unique, especially for D_{EO} around 1 μm.

S.2. Combination of optical counter measurements

The combination of the size spectra measured by the PCASP, UHSAS, and Grimm was performed by examining their overlap over their common measurement size ranges. The combination was performed as follows. First, the measured size distributions were visually inspected to establish whether, at the calibration refractive index (m_{latex} = 1.59 -0i), the observations by the counters coincided on their common size range. This analysis was repeated after applying the geometric equivalence correction according to the refractive index (that is, on the size distributions expressed as a function of D_{EG}). When the difference between the particle number concentration measured by the two counters (at pairs) was lower than the sum of the absolute counting errors (√d*N* according to the Poisson statistics), the agreement was considered as satisfactory. A boundary diameter (D_{cover}) was then defined in the overlap zone to generate a new combined size distribution from the PCASP or UHSAS in the particle diameter range $D'_{EG} \leq D_{COVER}$ and the Grimm counter in the range $D''_{EG} \geq D_{COVER}$ (with D''_{EG} up to the AVIRAD inlet cut-off diameter), so that

$$\frac{dN_{tot}(D_{EG})}{dlogD_{EG}} = \frac{dN_{PCASP}(D'_{EG})}{dlogD'_{EG}} + \frac{dN_{Grimm}(D''_{EG})}{dlogD''_{EG}} \quad \textbf{(S1.a)}$$

$$\frac{dN_{tot}(D_{EG})}{dlogD_{EG}} = \frac{dN_{UHSAS}(D'_{EG})}{dlogD'_{EG}} + \frac{dN_{Grimm}(D''_{EG})}{dlogD''_{Eg}} \quad \textbf{(S1.b)}$$

Figure S4 shows a schematic representation of the combination between both size distributions.

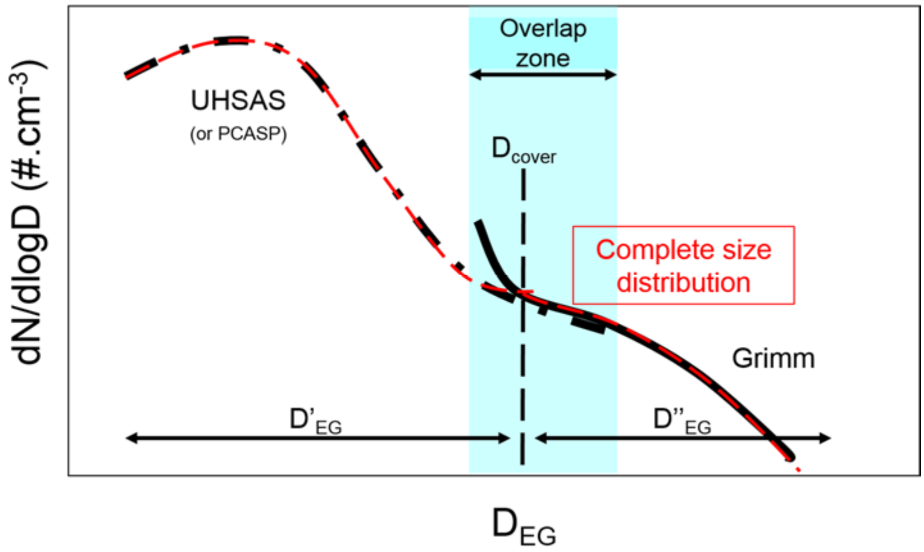

Figure S4. Schematics of the combination of the number size distributions between UHSAS (or PCASP) and Grimm around D_{cover}. The overlap zone is indicated in blue. The black curves represent the distributions measured by the two counters in pairs, corrected by the refractive index (e.g., expressed as D_{EG}). The red curves represent the combined size distributions of the two optical counters over the combination of the domain of D_{EG}' (for UHSAS or PCASP) and D_{EG}'' for the Grimm. In each diameter range below and over D_{COVER}, dlogD_{EG} values and counting errors remain those of the respective counter.

The overlapping zone changes whether we work with PCASP (TRAQA campaign) or UHSAS (ADRIMED campaign). D_{cover} ranged between 0.23 and 0.7 µm for the TRAQA campaign when the PCASP and the Grimm were operated, and between 0.23 and 0.9 µm during ADRIMED when the UHSAS and the Grimm were operated.

To make sure that the total number of particles was conserved after the recombination and the modification of the size classes by the refractive index, we applied the conservation equation of the total number of particles

$$N_{EG} = N_{EO} \quad \textbf{(S2.a)}$$

$$N_{EO} = \int_{D_{EO,min}}^{D_{EO,max}} \frac{dN_{EO}(D_{EO})}{dlogD_{EO}} dlogD_{EO} \quad \textbf{(S2.b)}$$

$$N_{EG} = \int_{D_{EG,min}}^{D_{EG,max}} \frac{dN_{EG}(D_{EG})}{dlogD_{EG}} dlogD_{EG} \qquad \textbf{(S2.c)}$$

where N_{EO} is the total number of particles corresponding to the measurement (for the refractive index m_{latex}) and N_{EG} is the total number of particles after correction of the refractive index.

Finally, the extended size distributions $\frac{dN_{EG}(D_{EG})}{dlogD_{EG}}$ obtained by the recombination of the optical particle counters were fitted by a multi modal normalized log-normal distributions as

$$\frac{1}{N_{EG}} \frac{dN_{EG}(D_{EG})}{dlogD_{EG}} = \sum_i \frac{n_i}{\sigma_i \sqrt{2\pi}} \exp\left(-\frac{\left(logD - logD_{0,i}\right)^2}{2\sigma_i^2}\right) \qquad \textbf{(S3)}$$

where n_i is the total number of particles, σ_i the geometric standard deviation and $D_{0,i}$ the modal (geometric mean) diameter of the mode *i*.

The log-normal fit of the reconstructed size distribution was done with the MPFIT routine available under IDL (Markwardt, 2009; http://purl.com/net/mpfit). The calculation routine considers the result as correct if the difference ε_{FIT} between the sum of the squares of the input size distribution and its deconvolution is less than 10^{-10} after 100 iterations. To limit error due to an over- or underestimation of the total number of particle N_{EG}, not constrained in this routine, the calculation was repeated several times, on normalized size distributions, by modifying the initial parameters until the calculated size distribution is within the limits of the counting uncertainties of the experimental size distributions. Examples of deconvolutions are shown in **Figure S5**.

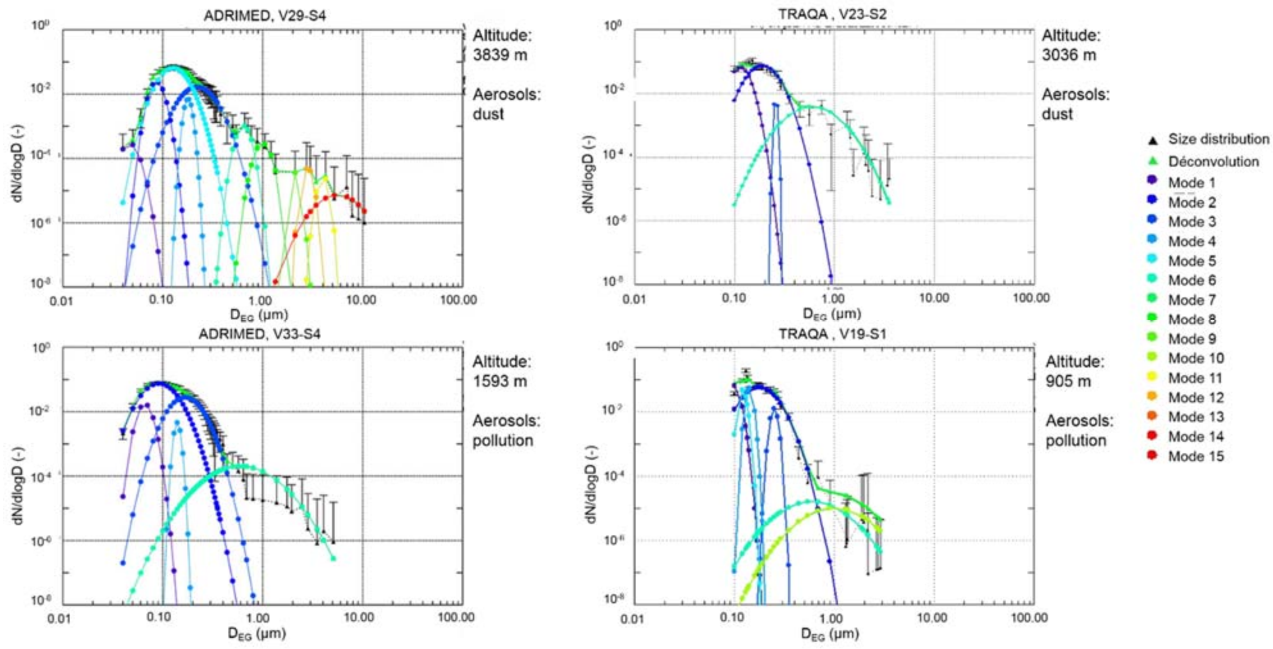

Figure S5. Examples of reconstructed normalized number size distributions and their decomposition in log-normal modes for case studies of desert dust (upper panels) and pollution aerosols (lower panels) during ADRIMED and TRAQA. The deconvolution was performed with the IDL MPFIT routine for up to 15 different log-normal distribution modes. The uncertainties correspond to the Poisson statistical error.

Up to 11 modes were needed to fit the size distributions, of which up to 6 modes for $D_{EG} < 1$ µm. These do not necessarily have a physical meaning but are regarded as a way of reproducing the volume distribution at the highest possible size resolution.

S.3. Assessment of the complex refractive index

The complex refractive index necessary to estimate D_{EG}, and therefore correct the measured size distributions according to the optical equivalent diameter D_{EO}, are based on published values in the literature, some of them especially for our region of study (Ackermann, 1998; Petzold et al., 2009; Ryder et al., 2013; Di Biagio et al., 2015; Denjean et al., 2016; Sicard et al., 2016). The different values are presented in **Table S2**.

Aerosol	Campaign	Wavelength (nm)	Refractive index	References
Pollution (fine mode)	TRAQA, SAFMED	632.8	(1.50 – 1.72) – *i* 0.01	*Di Biagio et al., 2015*
Pollution (soot)	---	355	1.75 – *i* 4.64 10^{-1}	*Ackermann, 1998*
		532	1.75 – *i* 4.46 10^{-1}	
		1064	1.76 – *i* 1.43 10^{-1}	
Marine	---	355	1.51 – *i* 3.22 10^{-8}	*Ackermann, 1998*
		532	1.50 – *i* 1.12 10^{-8}	
		1064	1.47 – *i* 1.92 10^{-4}	
Desert dust	---	355	1.53 – *i* 1.66 10^{-2}	*Ackermann, 1998*
		532	1.53 – *i* 6.33 10^{-3}	
		1064	1.53 – *i* 4.30 10^{-3}	
	ADRIMED	530	(1.51 – 1.57) – *i* (1.0 – 4.6) 10^{-3}	*Denjean et al., 2016*
	SAMUM	450	(1.55 – 1.57) – *i* (3.1 – 5.2) 10^{-3}	*Petzold et al., 2009*
		550	(1.55 – 1.56) – *i* (1.6 – 4.2) 10^{-3}	
		700	(1.55 – 1.56) – *i* (0.3 – 2.5) 10^{-3}	
	FENNEC	550	1.53 – *i* (1.0 – 3.0) 10^{-3}	*Ryder et al., 2013*
Mixed aerosols	AERONET	440	(1.42 – 1.48) – *i* (2.8 – 4.7) 10^{-3}	*Sicard et al., 2016*

Table S2. Compilation of published values of refractive index and their wavelengths, for different aerosol type with some of them especially for our region of study (Mediterranean Sea).

In the absence of complementary information on the variability of the chemical composition with size, the refractive index was considered as independent on particle size. The refractive index for mixed aerosols (AE_{scat} between 0.5 and 1.0) was calculated as volume-weighted averages of pollution aerosols and desert dust as

$$m = \sum_i f_i \times m_i \quad \textbf{(S4)}$$

where f_i et m_i are the volume fractions and the complex refractive index of two types of aerosols i, respectively. We assumed arbitrarily that f_i = 0.8 for desert dust and f_i = 0.2 for pollution aerosols for AE_{scat} ≤0.75, and f_i = 0.2 for desert dust and f_i = 0.8 for pollution aerosols for AE_{scat} >0.75. The extrapolation to our working wavelengths (450, 532, 550, 700 and 865 nm) was done by assuming the spectral dependences obtained by Ackermann (1998) between 355 and 532 nm and between 532 and and 1064 nm. The spectral dependence was applied to the refractive index for desert dust and mixed aerosols obtained by Di Biagio et al. (2016) and Denjean et al. (2016) for case studies during TRAQA and ADRIMED.

S.4. Comparison between in situ measurements and calculations of the extinction and scattering coefficient

The validation of the number size distributions reconstructed from airborne measurements, henceforth their ability in yielding the column-integrated but size-segregated extinction, was assessed by calculating, on 30-second averages, the extinction coefficient σ_{ext} at 532 nm and the scattering coefficient σ_{scat} at 450, 550 and 700 nm, and by comparing them to σ_{ext} measured by the CAPS-PMex (only operated during ADRIMED) and to σ_{scat} measured by the nephelometer, respectively. The comparisons were evaluated by examining the correlation coefficient R, the root-mean square error (RMS) and the bias (B) of their linear regression. The complex refractive index at each wavelength was varied until the best agreement between calculated and measured σ_{scat} and σ_{ext} was achieved within the estimated error bars. The retrieved refractive index matching measurements and calculations are summarized in **Table S3.**

Aerosol type	**Complex refractive index *m***								
	450 nm	**532 nm**	**550 nm**	**632.5 nm**	**655 nm**	**670 nm**	**700 nm**	**865 nm**	**1054 nm**
Clear layer / maritime	(1.40-1.50) -i(0 - 0.002)								
Desert dust	(1.50-1.57) – i(0.004-0.007)	(1.50-1.57) -i(0.002-0.004)						(1.50-1.57) – i(0.0020.003)	(1.50-1.57) – i(0.001-0.003)
Pollution	(1.41-1.77) – i(0.002-0.022)	(1.41-1.77) – i(0.002-0.018)	(1.41-1.77) – i(0.002-0.017)	(1.41-1.77) – i(0.002-0.015)	(1.41-1.77) -- i(0.002-0.014)	(1.41-1.77) – i(0.002-0.014)	(1.41-1.77) – i(0.002-0.013)	(1.42-1.78) – i(0.001-0.010)	(1.42-1.79) – i(0.001-0.008)
Mixed aerosol (AE ≤0.75)	(1.48-1.61) – i(0.004-0.010)	(1.48-1.61) – I(0.002-0.007)	(1.48-1.61) – i(0.002 - 0.007)	(1.48-1.61) – i(0.002-0.006)	(1.48-1.61) – i(0.002-0.006)	(1.48-1.61) – i(0.002-0.006)	(1.48-1.61) – i(0.002-0.005)	(1.48-1.61) – i(0.002-0.005)	(1.48-1.61) – i(0.002-0.004)
Mixed aerosol (*AE* >0.75)	(1.43-1.73) – i(0.002-0.019)	(1.43-1.73) – i(0.002-0.015)	(1.43-1.73) – i(0.002-0.014)	(1.43-1.73) – i(0.002-0.013)	(1.43-1.73) – i(0.002-0.012)	(1.43-1.73) – i(0.002-0.012)	(1.43-1.73) – i(0.002-0.011)	(1.43-1.73) – i(0.001-0.009)	(1.43-1.74) – i(0.001-0.007)

Table S3. Best-guess of the spectral refractive index obtained for the corrections of the optical particle counter, and comparison of measurements and calculations for clear layer/maritime aerosol, desert dust, pollution and mixed aerosol. The values extrapolated to 670 and 870 nm (working wavelengths of POLDER-3) are also shown.

The results of the comparison at 550 (σ_{scat}) and 532 nm (σ_{ext}) are illustrated in **Figure S6**. The uncertainties associated with the evaluation of the size distribution, the measured scattering and extinction, and finally the aerosol optical depth retrieved are estimated as the quadratic sum of the instrumental uncertainties as well as with the variability due to the reduction of the native time-resolution to a common time step of 30 seconds, a standard deviation generically indicated here as Δ_{30sec}. The instrumental uncertainties for the nephelometer and the CAPS-PMex are evaluated as ±10% for submicron aerosols (Anderson et al., 1996), and ±3.2% (Massoli et al., 2010), respectively. The error on the number of particles n_i (i = generic bin) follows the Poisson's law as $\Delta_{Poisson} = \sqrt{n_i}$. The comparison between measured and calculated σ_{scat} at 450 and 700 nm are not shown as they are analogous to those at 550 nm.

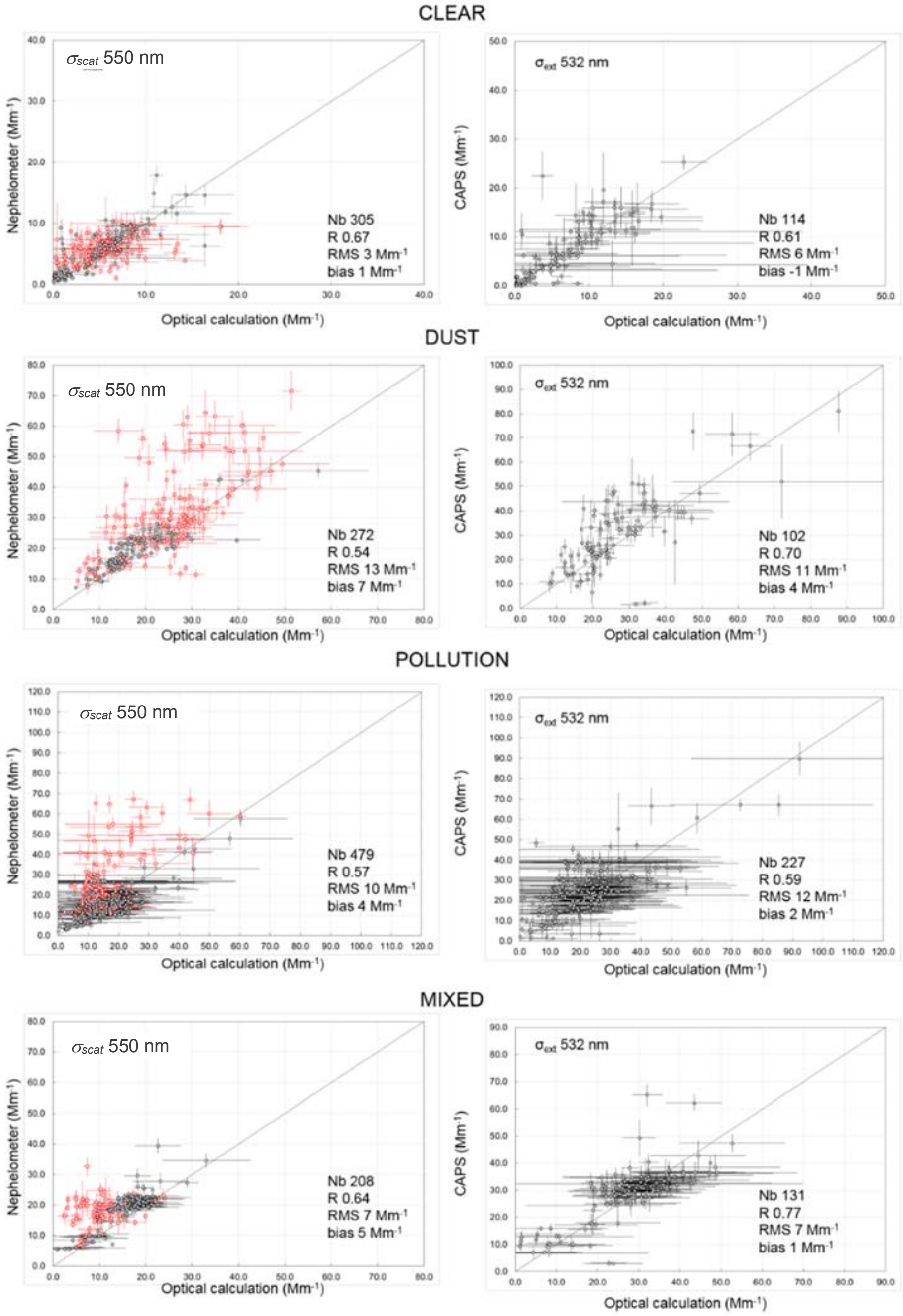

Figure S6. Comparison of optical calculation and measurements of σ_{scat} at 550 nm and σ_{ext} at 532 nm for all aerosol layers of all vertical profiles during TRAQA (red) and ADRIMED (black) campaigns. The comparison for σ_{ext} is shown only for ADRIMED since there were no CAPS-PMex measurements during TRAQA. See the text for error bars calculation.

The comparison is satisfactory for all aerosol types, and in particular concerning σ_{ext}. The systematic underestimation of the larger values of σ_{scat} during TRAQA is due to the faulty operation of the Grimm OPC above 350 m from sea level. These data points were removed from the dataset for POLDER-3 AOD and AOD_C evaluation while kept for the evaluation of

AOD_F which is not affected by errors in sizing the largest particles. The uncertainties for the optical computation of σ_{scat} are higher for pollution layers than for other types of aerosols. This is due to the wide range of possible values of the refractive index.